

# From OTFS to AFDM: A Comparative Study of Next-Generation Waveforms for ISAC in Doubly-Dispersive Channels

Hyeon Seok Rou, *Graduate Student Member, IEEE*,

Giuseppe Thadeu Freitas de Abreu, *Senior Member, IEEE*, Junil Choi, *Senior Member, IEEE*,

David González G., *Senior Member, IEEE*, Marios Kountouris, *Fellow, IEEE*,

Yong Liang Guan, *Senior Member, IEEE*, and Osvaldo Gonsa.

## Abstract

Next-generation wireless systems will offer integrated sensing and communications (ISAC) functionalities not only in order to enable new applications, but also as a means to mitigate challenges such as doubly-dispersive channels, which arise in high mobility scenarios and/or at millimeter-wave (mmWave) and Terahertz (THz) bands. An emerging approach to accomplish these goals is the design of new waveforms, which draw from the inherent relationship between the doubly-dispersive nature of time-variant (TV) channels and the environmental features of scatterers manifested in the form of multipath delays and Doppler shifts. Examples of such waveforms are the delay-Doppler domain orthogonal time frequency space (OTFS) and the recently proposed chirp domain affine frequency division multiplexing (AFDM), both of which seek to simultaneously combat the detrimental effects of double selectivity and exploit them for the estimation (or sensing) of environmental information. This article aims to provide a consolidated and comprehensive overview of the signal processing techniques required to support reliable ISAC over doubly-dispersive channels in beyond fifth generation (B5G)/sixth generation (6G) systems, with an emphasis on OTFS and AFDM waveforms, as those, together with the traditional orthogonal frequency division multiplexing (OFDM) waveform, suffice to elaborate on the most relevant properties of the trend. The analysis shows that OTFS and AFDM indeed enable significantly improved robustness against inter-carrier interference (ICI) arising from Doppler shifts compared to OFDM. In addition, the inherent delay-Doppler domain orthogonality of the OTFS and AFDM effective channels is found to provide significant advantages for the design and the performance of integrated sensing functionalities.

## I. INTRODUCTION

It is expected that beyond fifth generation (B5G) and sixth generation (6G) wireless systems will employ extremely high-frequency (EHF) technologies, operating in the millimeter-wave (mmWave) and Terahertz (THz) bands [1] as a means to support applications [2], such as Internet-of-Things (IoT), edge computing and smart cities; and scenarios such as vehicle-to-everything (V2X), high-speed rail, and non-terrestrial networks (NTNs), which are often subjected to heterogeneous and high-mobility conditions [3]. High-mobility scenarios are known to pose a significant challenge to wireless communications systems due to the resulting doubly-dispersive wireless channel, also referred to as time-variant (TV) multipath, or time-frequency selectivity [4]. Such heterogeneous scattering environments deteriorate the received signal in the form of path delays and Doppler shifts, resulting in inter-symbol interference (ISI) and inter-carrier interference (ICI) which can drastically decrease communication performance under conventional and highly effective modulation schemes, such as orthogonal frequency division multiplexing (OFDM) [5].

Concomitant with this challenge, there is a growing expectation that B5G and 6G systems will offer integrated sensing and communications (ISAC) capabilities, possibly with unified hardware and signal processing techniques [6]. In addition to providing environment perception and accurate/reliable localization information to serve the aforementioned applications, the enhancements introduced by ISAC are fundamental to improve spectrum and energy efficiency, and to lower hardware costs of systems operating in high-mobility scenarios [3].

While it is difficult to foresee which of the upcoming generations/standards – *i.e.*, B5G or 6G – will see ISAC adopted and implemented into commercial systems, the topic is one of the most intensively discussed among pre-standardization fora on wireless systems in recent years<sup>1</sup>, with notable examples being the 6G Smart Networks and Services Industry Association (6G-IA), where ISAC has been identified as a priority technology for its members, and the 5G Automotive Association (5GAA), where ISAC is considered an enabling technology for Cellular-V2X (C-V2X) services. Although it is reasonable to anticipate that any form of practically deployed 5G-based ISAC will likely leverage OFDM, more specifically cyclic prefix (CP)-OFDM and DFT-spread OFDM (DFT-s-OFDM) for downlink/sidelink, and uplink, respectively, but for 6G, new waveforms, such as orthogonal time frequency space (OTFS) and affine frequency division multiplexing (AFDM), should be considered to fully enable the potential of ISAC, as will be investigated in this article. In fact, important standardization bodies such as European Telecommunications Standards Institute (ETSI) and the 3<sup>rd</sup> generation partnership project (3GPP), which produce technical specifications for mobile broadband systems worldwide, have recently added ISAC to their work plans and roadmaps, with ETSI launching a new group dedicated to ISAC in November 2023.

<sup>1</sup>See <https://5gaa.org/> and <https://6g-ia.eu/> for additional information on 5GAA and 6G-IA, respectively.

In line with this trend, novel waveforms have been recently proposed which, thanks to their ability to retain symbol orthogonality under doubly-dispersive conditions, are both robust to high-mobility and advantageous for ISAC, as they inherently enable the estimation of environmental parameters, such as distance and velocity of scatterer objects (*i.e.*, delay and Doppler shifts). One of the most popular methods is OTFS signaling [7], which leverages the inverse symplectic finite Fourier transform (ISFFT) in order to modulate a two-dimensional (2D) grid of information symbols directly in the delay-Doppler domain, gaining great attention for high-mobility B5G systems thanks to its superior performance compared to currently used waveforms such as OFDM [8].

It is easy to show, indeed, that the full delay-Doppler representation of the channel in OTFS inherently conveys the velocity and range information of the scatterers in the form of the respective multipath delays and Doppler shifts, thus implying significant benefits in terms of ISAC. As a consequence, a plethora of OTFS-based ISAC techniques have been proposed to extract the delay and Doppler parameters of the resolvable paths directly from the channel state information (CSI), which have been shown to compete with the sensing performances of OFDM and frequency modulated continuous wave (FMCW) radars, with higher robustness to mobility and achievable capacity [9].

An alternative strategy to design ISAC-friendly and mobility-robust waveforms is to employ chirp-based multicarrier approaches [10]. While the chirp-domain design is attractive due to the inherent spread-spectrum property and potential for full-duplex operations, an important and common drawback of these earlier approaches is the lack of adaptability to the channel delay and Doppler spreads, which is a consequence of the non-parametrizable transforms in their design.

A more recent take on the idea, which seeks to mitigate the latter drawback, is the AFDM waveform [11], which leverages the inverse discrete affine Fourier transform (IDAFT) [12] in order to modulate information symbols into a *twisted* time-frequency domain, yielding the desired delay-Doppler orthogonality while maintaining the necessary flexibility. The optimizable parametrization of AFDM is further accompanied by other desirable properties, such as full diversity guarantee and increased throughput [11], making AFDM a strong candidate of ISAC-enabling waveform for B5G and 6G systems.

This article aims to offer a thorough analysis of the fundamentals and the future of ISAC technology in heterogeneous high-mobility scenarios, in the form of a comprehensive comparison of prominent candidate waveforms, focusing on OTFS and AFDM. The analysis reveals that the novel delay-Doppler orthogonal designs of OTFS and AFDM benefit the signal processing for both communication and sensing functionalities, advocating the integration of the two. These insights may hold significant interest and value not only for academia, but also for standardization engineers across various industry verticals who are increasingly participating in the development of future generations of mobile broadband systems.

The remainder of the article is organized as follows: the fundamental system models and the required ISAC signal processing techniques for the doubly-dispersive wireless channel<sup>2</sup>, emphasizing the inherent transformations between time, frequency, delay, and Doppler dimensions, are described in Section II. In Section III, the signal models of the identified candidate waveforms for B5G/6G ISAC in doubly-dispersive environments are consolidated, highlighting their interrelationships in terms of the multiplexing domain, transmitter structure, and the core *linear canonical transform (LCT)*. In Section IV, we discuss the radar sensing techniques leveraging the identified candidate waveforms in terms of the radar target detection problem (DP) and radar parameter estimation problem (EP), elaborating on signal processing techniques and solutions categorized into correlation-based methods, and direct/indirect CSI-based approaches. In Section V, the candidate waveforms are compared with basis on different key performance indicators (KPIs) for both communications and radar sensing performances, in addition to implications onto hardware implementation, requirements, and potential challenges. Finally, the key insights provided by the article are summarized, and some future directions of the research are identified.

## II. SIGNAL PROCESSING FUNDAMENTALS OF DOUBLY-DISPERSIVE CHANNELS

A long history of research on wireless communications has resulted in the identification and characterization of two fundamental and distinct types of small-scale fading effects, namely frequency- and time-selectivity, also known as time and frequency dispersion, respectively. In particular, an electromagnetic (EM) signal propagated through a given path is subject to a specific *path delay* proportional to the total propagation distance between the transmitter and the receiver, and a *Doppler shift*<sup>3</sup> proportional to the relative velocities among transmitter, receiver, and scatterer, and the carrier frequency.

In a channel with multiple distinguishable propagation paths, the different copies of the originally transmitted signal with varying time delays and Doppler shifts are superposed at the receiver, resulting in interference that impacts on the reliability and performance of the wireless communication link, unless appropriate signal processing techniques are employed. In this section, we first consolidate the fundamental doubly-dispersive channel model with all of its representations in the time, frequency, delay, and Doppler domains, along with the associated transformation methods, followed by the corresponding signal processing mechanisms available to process the received signal, by the efficient representation of the input-output relationship leveraging a circular convolution matrix.

<sup>2</sup>The importance of modelling the doubly-dispersive channel, especially for ISAC applications, is a highly relevant problem currently discussed in both academia and standardization [13].

<sup>3</sup>We remark that in the related literature, and therefore also in this article, the term *Doppler shift* is often used in a broad sense, including spectral shifts of the propagated signal resulting from phenomena other than the actual Doppler effect, such as frequency offsets and low-frequency phase noise at the local oscillators.

### A. The Doubly-Dispersive Channel Model

Consider a wireless channel between a transmitter and receiver which is modelled via  $P$  significant propagation paths, where each  $p$ -th resolvable path, with  $p \in \{1, \dots, P\}$ , is respectively described by a corresponding complex fading coefficient  $h_p \in \mathbb{C}$ , path delay  $\tau_p \in [0, \tau^{\max}]$ , and Doppler shift  $\nu_p \in [-\nu^{\max}, +\nu^{\max}]$ . The corresponding delay and Doppler spreads of such a doubly-dispersive channel are characterized by the maximum delay  $\tau^{\max}$  [s] and the maximum Doppler shift  $\pm\nu^{\max}$  [Hz], such that the channel can be described by the linear time-variant (LTV)<sup>4</sup> relationship between the input and the output signals. The LTV channel is most commonly represented as a time-variant impulse response function (TVIRF) in the time-delay domain, given by

$$h(t, \tau) \triangleq \sum_{p=1}^P h_p \cdot e^{j2\pi\nu_p t} \cdot \delta(\tau - \tau_p), \quad (1)$$

where  $j \triangleq \sqrt{-1}$  is the elementary imaginary number,  $t$  and  $\tau$  denote the instantaneous time and path delay, respectively, and  $\delta(x)$  is the unit impulse function defined by  $\delta(x) = 1$  iff  $x = 0$ .

Alternatively, the TVIRF in the time-delay domain can also be represented in other domains by leveraging appropriate linear transforms [12]. For example, the representation in the time-frequency domain is known as time-variant transfer function (TVTF), which is obtained by a Fourier transform (FT) on the TVIRF over the delay domain, *i.e.*,

$$H(t, f) \triangleq \mathcal{F}_{\tau \rightarrow f}[h(t, \tau)] = \int_{-\infty}^{+\infty} h(t, \tau) \cdot e^{-j2\pi\tau f} d\tau = \sum_{p=1}^P h_p \cdot e^{j2\pi\nu_p t} \cdot e^{-j2\pi\tau_p f}, \quad (2)$$

where  $f$  is the instantaneous frequency and  $\mathcal{F}[\cdot]$  denotes the continuous FT operator.

The TVTF in the time-frequency domain readily highlights both time and frequency dispersion effects of the channel, visible in the two fast-varying exponential terms dependent on the instantaneous time  $t$  and instantaneous frequency  $f$ , respectively at a rate of the Doppler frequency  $\nu_p$  and delay  $\tau_p$  of the corresponding  $p$ -th propagation path, as illustrated in Fig. 1a. Conversely, the Doppler-variant impulse response function (DVIRF) in the delay-Doppler domain is obtained by an FT on the TVIRF over the time domain, that is

$$\gamma(\nu, \tau) \triangleq \mathcal{F}_{t \rightarrow \nu}[h(t, \tau)] = \int_{-\infty}^{+\infty} h(t, \tau) \cdot e^{-j2\pi\nu t} dt = \sum_{p=1}^P h_p \cdot \delta(\nu - \nu_p) \cdot \delta(\tau - \tau_p), \quad (3)$$

where the time- and frequency-selectivity characteristics are observed in the form of unique impulses in the delay-Doppler plane corresponding to each propagation path, as illustrated in Fig. 1b.

<sup>4</sup>The term "linear time-variant (LTV) system" is not to be confused with linear systems with *time-varying delays* – *i.e.*, systems with delay drifts, where  $\tau_p(t)$  – which are also commonly described as LTV. In this article, we only consider time-invariant delays, in compliance with the related literature on doubly-dispersive channels, *e.g.*, [4], [7], [11].

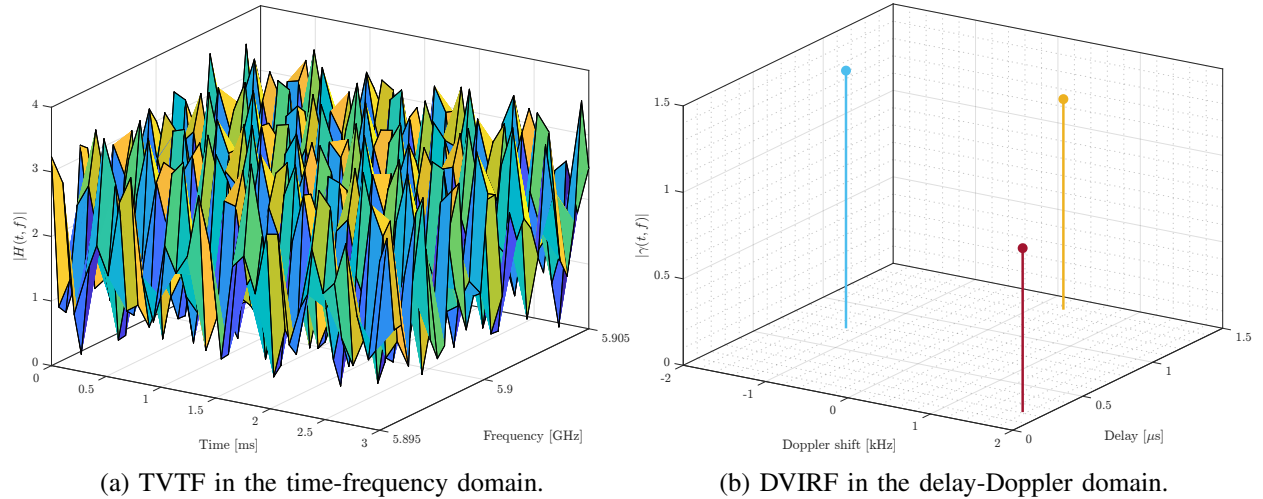


Fig. 1: The doubly-dispersive channel representations with  $P = 3$  resolvable paths, with carrier frequency of 5.9 GHz and signal bandwidth of 10 MHz (following the IEEE 802.11p vehicular environment specifications). The different paths are illustrated by unique colors in Fig. 1b.

It is important to note that the equivalent channel models in eqs. (1) - (3) are based on a practical approximation of the true doubly-dispersive wireless channel, represented in terms of a finite number of significant delay and Doppler frequency taps<sup>5</sup>, which is known to generally work well [4], [14] especially under the underspread environment assumption, *i.e.*, the maximum delay spread  $\tau_{\max} - \tau_{\min}$  is smaller than  $T$ , the maximum Doppler spread  $\nu_{\max} - \nu_{\min}$  is smaller than  $\frac{1}{T}$ , and  $\tau_{\max}\nu_{\max} \ll 1$ , where  $T$  is the finite signal period in seconds.

Following the above, Fig. 2 provides a diagram that summarizes the relationships between the various signal domains, including the direction and the integral domain of the necessary linear transforms. Specifically, the rhombus-shaped relationship at the center of the figure illustrates the different domain representations of the doubly-dispersive channel as described above, which also includes the omitted Doppler-variant transfer function (DVTF)<sup>6</sup> in the Doppler-frequency domain.

The Wigner transform (WT) and the Heisenberg transform (HT) (illustrated in red) are generalizations of the multiplexing (MX) and demultiplexing (DMX) operations of the classical OFDM modulator, which transform a 2D time-frequency domain signal into the single time and frequency domains. As will be discussed in the following section, the two transforms can be respectively implemented using the discrete Fourier transform (DFT) and the inverse discrete Fourier transform (IDFT). Furthermore, as can be seen

<sup>5</sup>Strictly speaking, a doubly-dispersive channel cannot be represented by both finite delay and Doppler taps, due to the incompatibility of the bandwidth-limited assumption and the temporally-limited assumption of the signals. Still, the approximation is well adopted in relevant research and studies [11], [14].

<sup>6</sup>The Doppler-frequency domain DVTF is not addressed as often compared to the other three forms, due to its lesser intuitive relationship with the physical phenomena. However, it is still an equally valid representation of the doubly-dispersive channel.

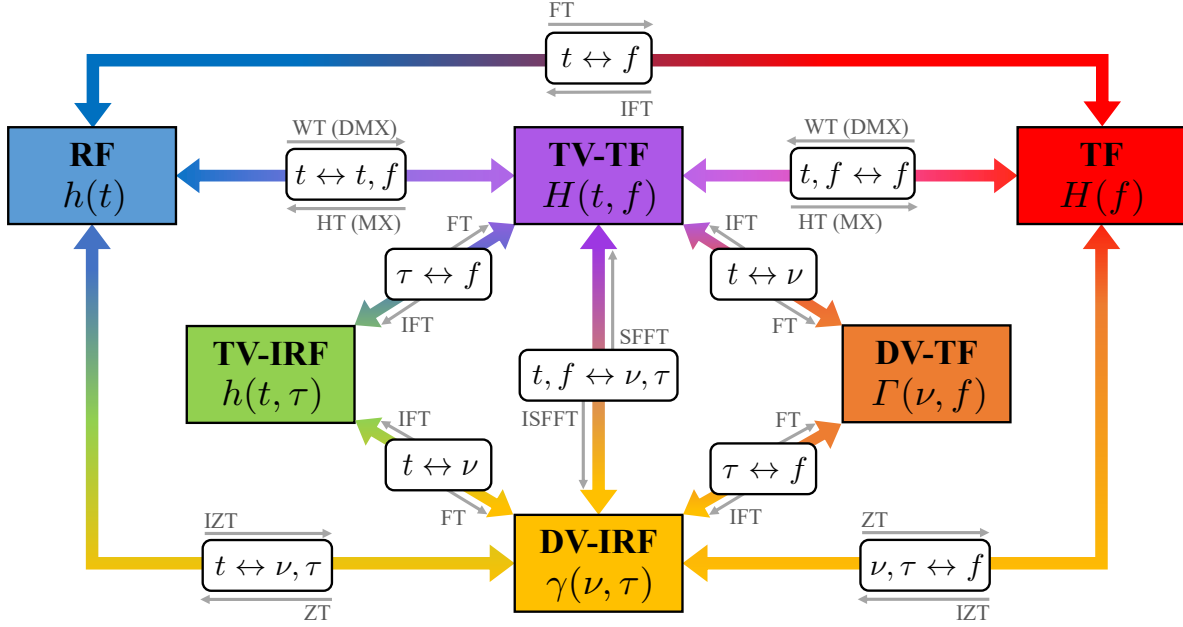


Fig. 2: Illustration of the relationship between the different signal domains and inherent transforms. In addition to the illustrated domains, a special case of the time-frequency domain, namely the **chirp domain**, also exists, which is omitted in this diagram but elaborated upon in the following sections.

in the figure, there also exist linear transforms that directly describe concatenated FTs and/or inverse Fourier transforms (IFTs). Such linear transforms, such as the symplectic finite Fourier transform (SFFT) and Zak transform (ZT), are leveraged in the transmitter design of next-generation waveforms such as the OTFS [7], and are elaborated in Sec. III.

To wrap up the signal domain fundamentals, let us also address the linear canonical transform (LCT) [12], also known as the affine Fourier transform (AFT), which is a four-parameter transform generalizing<sup>7</sup> many of the popular transforms such as the FT, Laplace transform (LT), and Fresnel transform (fnT).

In particular, the AFT  $\mathcal{L}_{t \rightarrow u}[\cdot]$  of a time-domain signal  $s(t)$  is described by

$$\mathcal{L}_{t \rightarrow u}[s(t)] \triangleq \begin{cases} \int_{-\infty}^{+\infty} s(t) \cdot \frac{1}{\sqrt{2\pi|b|}} \cdot e^{-j(\frac{a}{2b}u^2 + \frac{1}{b}ut + \frac{d}{2b}t^2)} dt, & b \neq 0, \\ s(d \cdot u) \cdot \frac{1}{\sqrt{a}} \cdot e^{-j\frac{cd}{2}u^2} & b = 0, \end{cases} \quad (4)$$

where the four AFT parameters  $(a, b, c, d)$  are arbitrary complex scalars satisfying  $ad - bc = 1$ .

As shall be seen, the available degrees-of-freedom (DoF)s of the AFT are exploited by another promising waveform, AFDM [11], which allows for the optimization of the AFT parameters based on the channel statistics in order to ensure the orthogonality of the signal in doubly-dispersive systems.

<sup>7</sup>Setting specific parameters reduces the LCT to the classical transforms such as  $(0, \frac{1}{2\pi}, -2\pi, 0)$  for the FT,  $(0, \frac{j}{2\pi}, j2\pi, 0)$  for the Laplace transform (LT), and  $(\cos\theta, \frac{1}{2\pi}\sin\theta, -2\pi\sin\theta, \cos\theta)$  to yield the  $\theta$ -th order fractional Fourier transform (frFT).

### B. Input-Output Relationship of Doubly-Dispersive Channel

The received signal model over the doubly-dispersive wireless channel  $h(t, \tau)$  in response to a time-domain transmit signal  $s(t)$  with bandwidth  $B$ , is classically described by the linear convolution over the delay domain leveraging the TVIRF representation [4], [14], namely

$$r(t) = s(t) * h(t, \tau) + w(t) \triangleq \int_{-\infty}^{+\infty} s(t - \tau) \left( \sum_{p=1}^P h_p \cdot e^{j2\pi\nu_p t} \cdot \delta(\tau - \tau_p) \right) d\tau + w(t), \quad (5)$$

where  $r(t)$  and  $w(t)$  are respectively the received signal and additive white Gaussian noise (AWGN) in time, while  $*$  denotes the linear convolution operator.

In turn, assuming that the channel and the AWGN are also bandlimited by bandwidth  $B$  of the transmit signal, sampling eq. (5) at a sampling rate of  $f_s \triangleq \frac{1}{T_s}$  [Hz] yields the discretized equivalent signal

$$r(nT_s) = \sum_{\ell=0}^{\infty} s(nT_s - \ell T_s) \left( \sum_{p=1}^P h_p \cdot e^{j2\pi\nu_p nT_s} \cdot \text{sinc}\left(\ell - \frac{\tau_p}{T_s}\right) \right) + w[n], \quad (6)$$

where  $n \in \{0, \dots, N-1\}$  and  $\ell \in \{0, \dots, N-1\}$  are the discrete time and delay indices,  $T_s$  [s] is the sampling period, and  $\text{sinc}(x) \triangleq \frac{\sin(\pi x)}{\pi x}$  is the normalized sinc function.

The presence of sinc functions resulting from sampling with a finite spectral support can result in interference between the Doppler responses between unique delay taps. However, assuming a wideband communication system as expected in the considered B5G and 6G scenarios, and in aid of oversampling if necessary, the sampling rate  $f_s$  will be sufficiently high such that the normalized path delays  $\ell_p \triangleq \tau_p f_s = \frac{\tau_p}{T_s}$  can be rounded to the nearest integer with negligible error, *i.e.*,  $\ell_p - \lfloor \frac{\tau_p}{T_s} \rfloor \approx 0$ , or in other words, the sampling resolution  $T_s$  is assumed to be sufficiently high such that the normalized path delays  $\ell_p$  are integers [7], [11], [14]. Consequently, the sinc functions are then actually equivalent to unit impulse functions<sup>8</sup>, such that eq. (6) can be expressed in terms of the sampled sequences

$$r[n] = \sum_{\ell=0}^{\infty} s[n - \ell] \left( \sum_{p=1}^P h_p \cdot e^{j2\pi f_p \frac{n}{N}} \cdot \delta[\ell - \ell_p] \right) + w[n], \quad (7)$$

where  $r[n]$ ,  $s[n]$ , and  $w[n]$  are respectively the sampled sequences of  $r(t)$ ,  $s(t)$ , and  $w(t)$ ;  $f_p \triangleq \frac{N\nu_p}{f_s} \in \left[-\frac{N\nu_{\max}}{f_s}, \frac{N\nu_{\max}}{f_s}\right]$  is the normalized digital Doppler shift of the  $p$ -th path;  $\ell_p \triangleq \frac{\tau_p}{T_s} \in \{0, \dots, \ell_{\max}\}$  is the normalized integer delay of the  $p$ -th path; and  $\delta[\cdot]$  is the discrete unit impulse function.

In addition, in practical multicarrier wireless communications techniques, the transmit sequence in eq. (7) is prepended with a cyclic prefix (CP) to mitigate the effects of time dispersion. The prefix sequence

<sup>8</sup>Given that the normalized path delays  $\ell_p$  are only integer-valued, the sinc functions which take integer input  $(\ell - \ell_p) \in \mathbb{N}_0$ , yield a value of 1 iff  $\ell - \ell_p = 0$ , and a value of 0 otherwise – this is equivalent to the discrete unit impulse function  $\delta[\ell - \ell_p]$ .



is defined within a CP length of  $N_{\text{cp}}$  samples, with  $N_{\text{cp}} \geq \ell_{\text{max}}$  such that

$$s[n'] = s[N + n'] \cdot e^{j2\pi \cdot \phi_{\text{cp}}(n')}, \quad (8)$$

where  $n' \in \{-1, \dots, -N_{\text{cp}}\}$ , and  $\phi_{\text{cp}}(n')$  is a function denoting the multiplicative phase term specific for each waveform, which for example, is set to zero if the CP does not require a phase offset, as in the OFDM, or a chirp-based phase offset as in the AFDM as will be seen in the following sections.

The CP as described in eq. (8) enables the linear convolutional input-output relation of the TVIRF to be processed as a circular convolutional response. After removing the received signal parts corresponding to the CP, the circular convolutional input-output relationship can be described in matrix form as

$$\mathbf{r} \triangleq \mathbf{H} \cdot \mathbf{s} = \left( \sum_{p=1}^P \overbrace{h_p \cdot \Phi_p \cdot \mathbf{W}^{f_p} \cdot \mathbf{\Pi}^{\ell_p}}^{\triangleq \mathbf{H}_p \in \mathbb{C}^{N \times N}} \right) \cdot \mathbf{s} + \mathbf{w} = \left( \sum_{p=1}^P \mathbf{H}_p \right) \cdot \mathbf{s} + \mathbf{w} \in \mathbb{C}^{N \times 1}, \quad (9)$$

where  $\mathbf{r} \in \mathbb{C}^{N \times 1}$ ,  $\mathbf{s} \in \mathbb{C}^{N \times 1}$ , and  $\mathbf{w} \in \mathbb{C}^{N \times 1}$  are respectively the vectors representing the received signal, the transmit signal, and AWGN;  $\mathbf{H} \in \mathbb{C}^{N \times N}$  is the circular convolution effective channel matrix;  $\Phi_p \in \mathbb{C}^{N \times N}$  is the diagonal matrix corresponding to the  $p$ -th delayed CP phase as given in eq. (10);  $\mathbf{W} \in \mathbb{C}^{N \times N}$  is the diagonal matrix containing the  $N$ -th roots of unity as given in eq. (11) whose exponentiation by a real number is equivalent to the element-wise exponentiation of the diagonal elements; and  $\mathbf{\Pi} \in \mathbb{C}^{N \times N}$  is the forward cyclic shift matrix<sup>9</sup> obtained by left-shifting the  $N \times N$  identity matrix once, such that right-multiplying by  $\mathbf{\Pi}^{\ell_p}$  corresponds to a cyclic left-shift of a matrix by  $\ell_p \in \mathbb{N}_0$  elements.

As can be seen in eq. (9), the input-output relationship of a doubly-dispersive channel is described by a matrix  $\mathbf{H}$  consisting of  $P$  off-diagonals, whose shifted positions are determined by the integer delay of each path. In addition, the complex values along each diagonal contain the channel fading coefficient and the phase offset information of the delayed CP and the Doppler shift of each path. As a consequence of the circulant convolutional channel structure, the different paths are only resolvable in the delay domain and not in the Doppler domain. Therefore, a key design objective of a double-dispersion robust waveform must be the ability to orthogonalize the delays and Doppler shifts of the channel via means of novel domain transforms in the modulation and demodulation of the transmit signal.

---


$$\Phi_p \triangleq \text{diag} \left( \overbrace{\left[ e^{-j2\pi \cdot \phi_{\text{cp}}(\ell_p)}, e^{-j2\pi \cdot \phi_{\text{cp}}(\ell_p-1)}, \dots, e^{-j2\pi \cdot \phi_{\text{cp}}(2)}, e^{-j2\pi \cdot \phi_{\text{cp}}(1)} \right]}^{\ell_p \text{ terms}}, \overbrace{\left[ 1, 1, \dots, 1, 1 \right]}^{N-\ell_p \text{ ones}} \right) \in \mathbb{C}^{N \times N}. \quad (10)$$

$$\mathbf{W} \triangleq \text{diag} \left( \left[ 1, e^{-j2\pi/N}, \dots, e^{-j2\pi(N-2)/N}, e^{-j2\pi(N-1)/N} \right] \right) \in \mathbb{C}^{N \times N}. \quad (11)$$

<sup>9</sup>To clarify with an example of  $N = 3$ ,  $\mathbf{\Pi}^0 \equiv \mathbf{I}_3 = \begin{bmatrix} 1 & 0 & 0 \\ 0 & 1 & 0 \\ 0 & 0 & 1 \end{bmatrix}$ ,  $\mathbf{\Pi}^1 = \begin{bmatrix} 0 & 0 & 1 \\ 1 & 0 & 0 \\ 0 & 1 & 0 \end{bmatrix}$ , and  $\mathbf{\Pi}^2 = \begin{bmatrix} 0 & 1 & 0 \\ 0 & 0 & 1 \\ 1 & 0 & 0 \end{bmatrix}$ , and so on.

### C. MIMO System Model of Doubly-Dispersive Channels

Extending the single-input single-output (SISO) model of the doubly-dispersive channel and its received signal model to the multiple-input multiple-output (MIMO) scenario between a transmitter array equipped  $N_T$  antennas and a receiver array equipped with  $N_R$  antennas, the received signal  $\mathbf{r}_{n_r} \in \mathbb{C}^{N \times 1}$  at the  $n_r$ -th receive antenna, with  $n_r \in \{1, \dots, N_R\}$ , is given by

$$\mathbf{r}_{n_r} \triangleq \sum_{n_t=1}^{N_T} \mathbf{H}_{n_t, n_r} \cdot \mathbf{s}_{n_t} + \mathbf{w}_{n_r} = \sum_{n_t=1}^{N_T} \overbrace{\left( \sum_{p=1}^P h_{p, n_t, n_r} \cdot \Phi_p \cdot \mathbf{W}^{f_p} \cdot \mathbf{\Pi}^{\ell_p} \right)}^{\triangleq \mathbf{H}_{n_t, n_r}} \cdot \mathbf{s}_{n_t} + \mathbf{w}_{n_r} \in \mathbb{C}^{N \times 1}, \quad (12)$$

where  $\mathbf{H}_{n_t, n_r} \in \mathbb{C}^{N \times N}$  is the convolutional channel between the  $n_t$ -th transmit antenna and the  $n_r$ -th receive antenna, with  $n_t \in \{1, \dots, N_T\}$ ,  $\mathbf{s}_{n_t} \in \mathbb{C}^{N \times 1}$  is the transmit signal vector from the  $n_t$ -th transmit antenna,  $h_{p, n_t, n_r} \in \mathbb{C}$  is the complex channel fading coefficient corresponding to the propagation path between the  $n_t$ -th transmit antenna and the  $n_r$ -th receive antenna via the  $p$ -th scatterer, and  $\mathbf{w}_{n_r} \in \mathbb{C}^{N \times 1}$  is the AWGN vector at the  $n_r$ -th receive antenna.

Notice that the MIMO received signal model in eq. (12) inherently assumes that the path delays  $\ell_p$  and Doppler shifts  $f_p$  are not spatially dependent, *i.e.*, they are identical across all transmit and receive antenna pairs for each propagation path, in accordance to the state-of-the-art (SotA) standardization reports and literature [15]. Therefore, only the complex fading coefficients  $h_{p, n_t, n_r} \in \mathbb{C}$  are considered to be dependent on the specific  $p$ -th path between the  $n_t$ -th transmit antenna and the  $n_r$ -th receive antenna.

However, when beamforming is considered at the MIMO arrays, the effects of spatial filtering [16] introduce angle-dependent antenna gains at the transmitter and/or receiver, which may vary the visibility and hence the doubly-dispersive channel statistics. To this end, consider an arbitrary transmit beamformer and a receive beamformer applied at the MIMO transmitter and receiver, respectively, where the corresponding transmit beamforming gain at an angle-of-departure  $\theta^t$  be denoted by  $f(\theta^t)$ , and the receive beamforming gain at an angle-of-arrival  $\theta^r$  by  $g(\theta^r)$ . Then, the beamformed channel between the  $n_t$ -th transmit antenna and the  $n_r$ -th receive antenna is described by

$$\mathbf{H}_{n_t, n_r} = \sum_{p=1}^P g(\theta_p^r) \cdot f(\theta_p^t) \cdot h_{p, n_t, n_r} \cdot (\Phi_p \cdot \mathbf{W}^{f_p} \cdot \mathbf{\Pi}^{\ell_p}), \quad (13)$$

where  $\theta_p^t$  and  $\theta_p^r$  are the relative angle of the  $p$ -th scatterer to the transmitter and the receiver arrays<sup>10</sup>.

Due to the "direction"-dependent gains of the transmit and receive beamformers for each path, it is implied that a given scatterer and its doubly-dispersive propagation path is only visible to the channel if it is within the angular range of the major beam. Consequently, the presence of certain scattering

<sup>10</sup>This model can be generalized to 2D planar arrays incorporating the azimuth and elevation angles of arrival and departure.

paths may be rendered negligible, such that for MIMO systems, the doubly-dispersive channel statistics including delay spread, Doppler spread, and the number of significant paths, are beamspace-dependent.

### III. SIGNAL MODELS OF NEXT-GENERATION WAVEFORMS

In this section, we provide the signal models and the transmitter structures of the various waveforms proposed for high performance in the doubly-dispersive channel. First, the OFDM waveform is described as a reference, followed by the next-generation waveform candidates, namely, OTFS, and AFDM, in addition to various derivative waveforms that can be related to the latter<sup>11</sup>.

#### A. Orthogonal Frequency Division Multiplexing (OFDM)

The well-known OFDM transmitter modulates digital symbols from the frequency domain into a time domain signal employing an IDFT operation, as illustrated in Fig. 2. Namely, given a vector  $\mathbf{x} \in \mathbb{C}^{N \times 1}$  consisting of  $N$  complex symbols, the OFDM transmit signal  $\mathbf{s}^{\text{OFDM}} \in \mathbb{C}^{N \times 1}$  is given by [17]

$$\mathbf{s}^{\text{OFDM}} = \mathbf{F}_N^{-1} \cdot \mathbf{x} \in \mathbb{C}^{N \times 1}, \quad (14)$$

where  $\mathbf{F}_N \in \mathbb{C}^{N \times N}$  is the  $N$ -point DFT matrix, and hence  $\mathbf{F}_N^{-1} \triangleq \mathbf{F}_N^H$  is the  $N$ -point IDFT matrix.

Following the above, the received signal  $\mathbf{y}^{\text{OFDM}} \in \mathbb{C}^{N \times 1}$  over the circular convolutional channel described by eq. (9) is demodulated via the forward  $N$ -point DFT, *i.e.*,

$$\mathbf{y}^{\text{OFDM}} = \mathbf{F}_N \underbrace{(\mathbf{H} \cdot \mathbf{s}^{\text{OFDM}} + \mathbf{w})}_{\triangleq \mathbf{r}^{\text{OFDM}} \in \mathbb{C}^{N \times 1}} = \underbrace{(\mathbf{F}_N \cdot \mathbf{H} \cdot \mathbf{F}_N^H)}_{\triangleq \mathbf{G}^{\text{OFDM}} \in \mathbb{C}^{N \times N}} \mathbf{x} + \mathbf{F}_N \cdot \mathbf{w} \in \mathbb{C}^{N \times 1}, \quad (15)$$

where, for exposition convenience, we defined the OFDM receive signal as  $\mathbf{r}^{\text{OFDM}} \in \mathbb{C}^{N \times 1}$ , and the effective channel  $\mathbf{G}^{\text{OFDM}} \in \mathbb{C}^{N \times N}$  describing the input-output relationship of the baseband OFDM symbols, which can be obtained by combining eqs. (9) and (15) to yield

$$\mathbf{G}^{\text{OFDM}} \triangleq \sum_{p=1}^P h_p \cdot \mathbf{F}_N (\mathbf{W}^{f_p} \cdot \mathbf{\Pi}^{\ell_p}) \mathbf{F}_N^H, \quad (16)$$

where the CP phase matrices  $\mathbf{\Phi}_p$  existent in eq. (9) have been reduced to identity matrices, as the CP of OFDM signals does not require a phase offset, *i.e.*,  $\phi_{\text{CP}}(n) = 0$  in eq. (10).

As illustrated in Fig. 3, the column-wise DFT and row-wise IDFT in presence of fractional normalized digital Doppler shifts cause the channel diagonals of the convolution matrix to be spread into a decaying band, centered at the original diagonals, such that significant interference between each path may arise.

<sup>11</sup>A Matlab<sup>®</sup> implementation of the doubly-dispersive channel model described in this section, as well as a convenient channel visualization tool used to generate some of the figures can be found our online repository [*here*].

## B. Orthogonal Time Frequency Space (OTFS)

In the OTFS modulation scheme, the information symbols are first directly placed in the delay-Doppler domain, instead of the frequency domain as in the OFDM approach, which are then multiplexed into the time signal. Namely, the complex baseband symbols are structured into a 2D grid of size  $K \times L$  in the delay-Doppler domain, which is transformed into a time-domain signal via the inverse discrete Zak transform (IDZT). Alternatively, as illustrated in Fig. 2, the equivalent<sup>12</sup> domain transform can be achieved via a two-step process, in which the delay-Doppler signal is first transformed into the time-frequency domain via the ISFFT, and then into the continuous time signal via a pulse-shaping HT.

This article will hereafter adopt the more common ISFFT formulation implemented via DFTs/IDFTs. In light of the above, the OTFS modulation process can be described mathematically as

$$\mathbf{s}^{\text{OTFS}} \triangleq \text{vec} \left( \overbrace{\mathbf{P}^{\text{tx}} \mathbf{F}_K^{-1}}^{\text{Pulse-shaping HT}} \cdot \overbrace{(\mathbf{F}_K \mathbf{X} \mathbf{F}_L^{-1})}^{\text{ISFFT}} \right) = (\mathbf{F}_L^{-1} \otimes \mathbf{P}^{\text{tx}}) \cdot \overbrace{\text{vec}(\mathbf{X})}^{\triangleq \mathbf{x}} \in \mathbb{C}^{KL \times 1}, \quad (17)$$

where  $\mathbf{s}^{\text{OTFS}} \in \mathbb{C}^{KL \times 1}$  is the OTFS transmit signal vector,  $\mathbf{X} \in \mathbb{C}^{K \times L}$  is the information symbol matrix consisting of  $N \triangleq KL$  number of complex symbols<sup>13</sup>,  $\mathbf{P}^{\text{tx}} \in \mathbb{C}^{K \times K}$  is the diagonal transmit pulse-shaping filter matrix<sup>14</sup>,  $\mathbf{F}_K \in \mathbb{C}^{K \times K}$  and  $\mathbf{F}_L \in \mathbb{C}^{L \times L}$  are the  $K$ -point and  $L$ -point DFT matrices, and  $\text{vec}(\cdot)$  and  $\otimes$  denote the stacking vectorization and Kronecker product operators, respectively.

The filtered and demodulated signal  $\mathbf{y}^{\text{OTFS}}$  after the convolution channel  $\mathbf{H}$  in eq. (9) is given by

$$\mathbf{y}^{\text{OTFS}} \triangleq (\mathbf{F}_L \otimes \mathbf{P}^{\text{rx}}) \overbrace{(\mathbf{H} \cdot \mathbf{s}^{\text{OTFS}} + \mathbf{w})}^{\triangleq \mathbf{r}^{\text{OTFS}} \in \mathbb{C}^{KL \times 1}} = \mathbf{G}^{\text{OTFS}} \cdot \mathbf{x} + (\mathbf{F}_L \otimes \mathbf{P}^{\text{rx}}) \cdot \mathbf{w} \in \mathbb{C}^{KL \times 1}, \quad (18)$$

where  $\mathbf{P}^{\text{rx}} \in \mathbb{C}^{K \times K}$  is the diagonal matched filter matrix of  $\mathbf{P}^{\text{tx}}$ , and the effective OTFS channel  $\mathbf{G}^{\text{OTFS}} \in \mathbb{C}^{N \times N}$  in the delay-Doppler domain is given by

$$\mathbf{G}^{\text{OTFS}} \triangleq \sum_{p=1}^P h_p \cdot (\mathbf{F}_L \otimes \mathbf{P}^{\text{rx}}) \left( \mathbf{W}^{f_p} \cdot \mathbf{\Pi}^{\ell_p} \right) (\mathbf{F}_L^H \otimes \mathbf{P}^{\text{tx}}) \in \mathbb{C}^{N \times N}, \quad (19)$$

which is the convolutional channel matrix  $\mathbf{H}$  after a block-wise pulse-shaped DFT and IDFT, and similarly to the OFDM waveform, the CP phase matrices  $\Phi_p$  have been reduced to identity matrices, as the OTFS signal also does not require a phase offset.

It can be observed from eq. (19) that the  $KL = N$  elements in each diagonal of the convolutional matrix of eq. (9) are spread into the OTFS effective channel via the block-wise pulse-shaping FTs, such that the

<sup>12</sup>While mathematically equivalent, in practice, the two-step SFFT-based transform process has been shown to exhibit higher Doppler leakage than the ZT-based counterpart, whose effect decreases with a larger number of subcarriers [18].

<sup>13</sup>Without loss of generality, we assume  $N \triangleq KL$  to enable direct comparison with 1D modulation schemes, *i.e.*, OFDM.

<sup>14</sup>The literature commonly assumes a non-ideal rectangular pulse-shape, which reduces  $\mathbf{P}^{\text{tx}}$  to a  $K \times K$  identity matrix. However, the specific design of the OTFS pulse-shaping function, in addition to the OTFS time-frequency windowing function [19], is an important design criteria for OTFS which must be addressed to improve the communications and sensing performance.

$KL \times KL$  OTFS channel matrix can be considered as a  $K \times K$  grid of  $L \times L$  sub-matrices (illustrated as minor grids in Fig. 3). In light of the above, the positions of the non-zero channel coefficient elements can be deterministically obtained by the values of both normalized delay and normalized digital Doppler of each path, respective to the occupied sub-matrices and the amount of left-shift of the diagonals.

If the normalized digital Doppler frequencies are integers, *i.e.*,  $f_p \in \mathbb{Z}$ , (not the true Doppler frequencies  $\nu_p$ ), each path occupies exactly  $K$  sub-matrices out of the  $K \times K$  grid in a shifted block-diagonal structure, whose amount of right-shift is determined by the integer component of the Doppler shift,  $f_p^{\text{int}} \triangleq \lfloor f_p \rfloor$ . For example, a path with  $f_p^{\text{int}} = 0$  occupies the  $K$  sub-matrices in the main block-diagonal (shift of index 0), whereas a path with  $f_p^{\text{int}} = 1$  occupies the  $K$  sub-matrices in the block-diagonal, which is right-shifted by an index of 1. On the other hand for negative Doppler shifts, the block-diagonals are left-shifted by an index of  $\lfloor f_p^{\text{int}} \rfloor$ , as illustrated by path 3 in Fig. 3a.

In turn, each of the  $K$  occupied sub-matrices follows the same structure consisting of exactly  $L$  non-zero elements in a shifted diagonal, with a left-shift relative to the main diagonal determined by the value of the normalized path delay  $\ell_p \in \mathbb{N}$ . For example, for a path with delay  $\ell_p = 0$ , the  $L$  non-zero elements are placed in the main diagonal for all  $K$  sub-matrices, whereas a path with  $\ell_p = 3$  will have the  $L$  non-zero elements in the diagonal left-shifted by three indices, for all  $K$  sub-matrices.

It follows that the OTFS waveform can achieve complete orthogonality and resolvability in the delay-Doppler domain assuming integer values of the normalized delay and normalized digital Doppler shifts, and if the channel satisfies the orthogonality condition given by  $\ell^{\max} \leq L - 1$  and  $f^{\max} \leq \lfloor \frac{K}{2} \rfloor$ , where  $\ell^{\max} \triangleq \lceil \frac{\tau^{\max}}{T_s} \rceil$  and  $f^{\max} \triangleq \lfloor \frac{N\nu^{\max}}{f_s} \rfloor$  are the maximum normalized delay and digital Doppler shift. Note that the orthogonality condition inherently implies that the OTFS waveform will remain orthogonal between unique paths even when the Doppler spread is negligible, *i.e.*,  $f^{\max} = 0$ , for fixed  $K$  and  $L$ .

In contrast, in the case of **fractional** values of normalized digital Doppler, *i.e.*,  $f_p \triangleq f_p^{\text{int}} + f_p^{\text{frac}} \in \mathbb{R}$ , where  $f_p^{\text{frac}} \in [0.5, +0.5)$ , the powers of the channel elements are diffused (or "leaked") across all  $K^2$  sub-matrices over the main  $K$  block-diagonal sub-matrices of the integer case, resulting in a Doppler domain interference as illustrated in Fig. 3b and Fig. 3c. The amount of such power leakage is determined by the magnitude of the fractional component of the normalized digital Doppler shift  $\lfloor f_p^{\text{frac}} \rfloor$ , such that larger magnitudes result in more leakage and hence a more severe interference.

### C. Affine Frequency Division Multiplexing (AFDM)

In AFDM, a one-dimensional vector of symbols  $\mathbf{x} \in \mathbb{C}^{N \times 1}$  is directly multiplexed into a *twisted* time-frequency chirp domain using the IDAFT [20], as described by

$$\mathbf{s}^{\text{AFDM}} \triangleq \mathbf{A}^{-1} \cdot \mathbf{x} = \overbrace{(\mathbf{\Lambda}_{c_2} \cdot \mathbf{F}_N \cdot \mathbf{\Lambda}_{c_1})^{-1}}^{\text{IDAFT}} \cdot \mathbf{x} = (\mathbf{\Lambda}_{c_1}^H \cdot \mathbf{F}_N^H \cdot \mathbf{\Lambda}_{c_2}^H) \cdot \mathbf{x} \in \mathbb{C}^{N \times 1}, \quad (20)$$

where  $\mathbf{A} \triangleq \mathbf{\Lambda}_{c_2} \mathbf{F}_N \mathbf{\Lambda}_{c_1} \in \mathbb{C}^{N \times N}$  is the forward  $N$ -point discrete affine Fourier transform (DAFT) matrix,  $\mathbf{\Lambda}_{c_i} \triangleq \text{diag}[e^{-j2\pi c_i(0)^2}, \dots, e^{-j2\pi c_i(N-1)^2}] \in \mathbb{C}^{N \times N}$  is a diagonal chirp matrix with a central digital frequency of  $c_i$ , and the central frequencies  $c_1$  and  $c_2$  of the two diagonal chirps<sup>15</sup> can be optimized to the channel statistics to improve the delay-Doppler orthogonality of the AFDM effective channel.

It follows that the demodulated AFDM signal over the convolution channel in eq. (9) is given by

$$\mathbf{y}^{\text{AFDM}} = \mathbf{A} \cdot \overbrace{(\mathbf{H} \cdot \mathbf{s}^{\text{AFDM}} + \mathbf{w})}^{\triangleq \mathbf{r}^{\text{AFDM}} \in \mathbb{C}^{N \times 1}} = \mathbf{G}^{\text{AFDM}} \cdot \mathbf{x} + \mathbf{A} \cdot \mathbf{w} \in \mathbb{C}^{N \times 1}, \quad (21)$$

with the effective AFDM channel given by

$$\mathbf{G}^{\text{AFDM}} \triangleq \sum_{p=1}^P h_p \cdot (\mathbf{\Lambda}_{c_2} \cdot \mathbf{F}_N \cdot \mathbf{\Lambda}_{c_1}) \left( \mathbf{\Phi}_p \cdot \mathbf{W}^{f_p} \cdot \mathbf{\Pi}^{\ell_p} \right) (\mathbf{\Lambda}_{c_1}^H \cdot \mathbf{F}_N^H \cdot \mathbf{\Lambda}_{c_2}^H) \in \mathbb{C}^{N \times N}, \quad (22)$$

where the CP phase matrices  $\mathbf{\Phi}_p$  require a chirp-cyclic phase offset, described by  $\phi_{\text{cp}}(n) = c_1(N^2 + 2Nn)$ , which in the specific case of even  $N$  and integer  $2Nc_1$ , reduces the matrices  $\mathbf{\Phi}_p$  back to identity.

The AFDM effective channel can also achieve full orthogonality in the integer normalized delay-Doppler domain when the channel satisfies the orthogonality condition, which is given by

$$2(f^{\max} + \xi)(\ell^{\max} + 1) + \ell^{\max} \leq N, \quad (23)$$

where  $f^{\max}$  and  $\ell^{\max}$  are the maximum normalized digital Doppler shift and delay of the channel,  $\xi \in \mathbb{N}_0$  is a free parameter determining the so-called *guard width* of the AFDM, denoting the number of additional guard elements around the diagonals to anticipate for Doppler-domain interference.

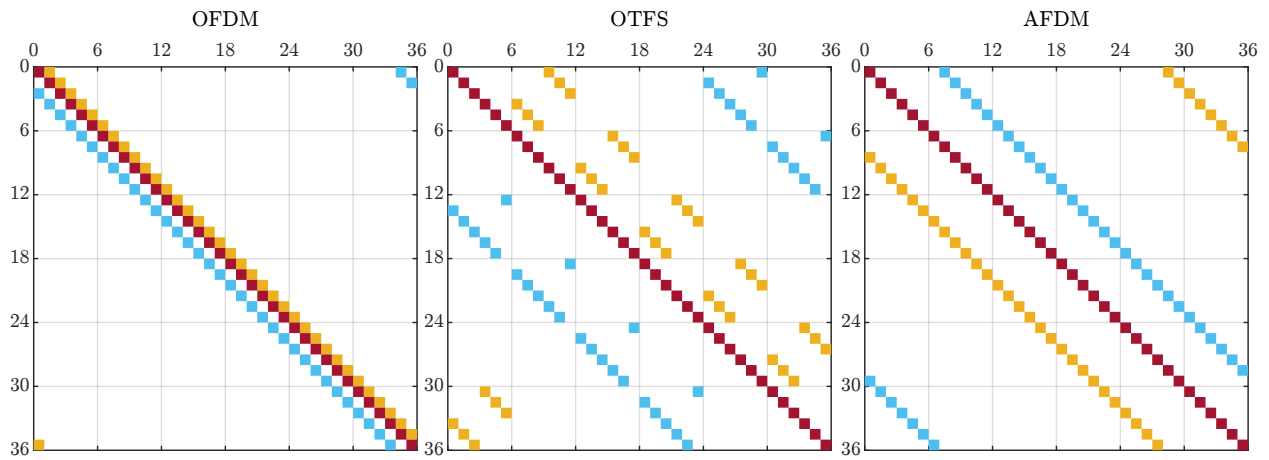
Assuming the orthogonality condition is met, the optimal AFDM chirp frequencies satisfy

$$c_1 = \frac{2(f^{\max} + \xi) + 1}{2N}, \quad \text{and} \quad c_2 \ll \frac{1}{N}, \quad (24)$$

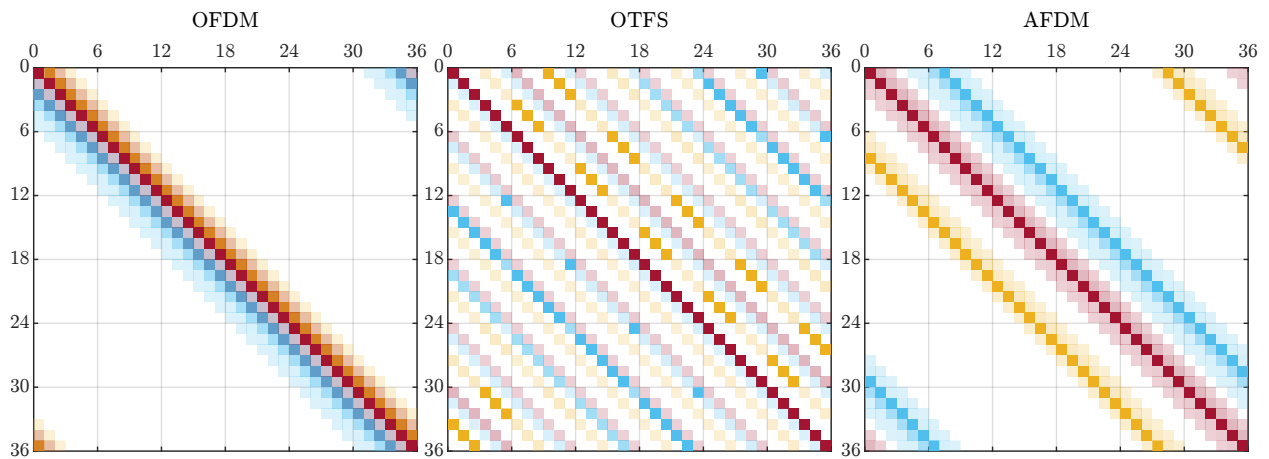
where the flexibility in  $c_2$  enables fine-tuning of the waveform shape as will be discussed in Sec. IV.

In light of the above, the position of the shifted diagonal in the AFDM channel can also be described in terms of the integer values of the normalized delay-Doppler indices of each path. Unlike the intricate block-wise structure of the OTFS effective channel, the AFDM effective channel exhibits only a single diagonal per path, which is shifted by a deterministic index dependent on the integer normalized delay  $\ell_p$  and integer normalized digital Doppler shift  $f_p^{\text{int}}$ . In other words, each diagonal of the convolution channel in eq. (9) is right-shifted by an index of exactly  $\ell_p \cdot 2(f^{\max} + \xi) + f_p^{\text{int}}$  positions, as illustrated in Fig. 3a. On the other hand, in the presence of fractional components of normalized digital Doppler shifts, the diagonals of the AFDM effective channels also exhibit a power leakage around the main diagonal, resulting in Doppler-domain interference as can be seen in Figs. 3b and 3c.

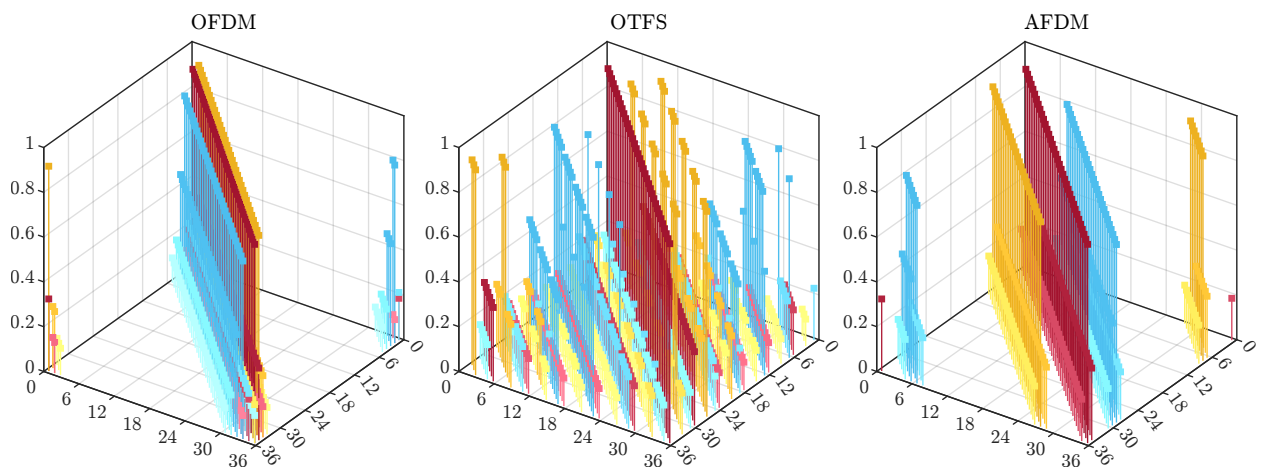
<sup>15</sup>It is shown in [11] that the chirp frequencies  $c_1$  and  $c_2$  are actually correspondent to the four configurable parameters of the AFT formulation in eq. (4).



(a) Target parameters:  $\{\ell_1=0, f_1=0\}$  (red),  $\{\ell_2=1, f_2=-2\}$  (blue),  $\{\ell_3=3, f_3=+1\}$  (yellow).



(b) Target parameters:  $\{\ell_1=0, f_1=0.266\}$  (red),  $\{\ell_2=1, f_2=-2.365\}$  (blue),  $\{\ell_3=3, f_3=+1.231\}$  (yellow).



(c) Target parameters:  $\{\ell_1=0, f_1=0.266\}$  (red),  $\{\ell_2=1, f_2=-2.365\}$  (blue),  $\{\ell_3=3, f_3=+1.231\}$  (yellow).

Fig. 3: Effective channel matrix structures of different waveforms in a doubly-dispersive channel with  $P = 3$  resolvable paths (each depicted in a different color), with corresponding normalized delays  $\ell_p$  and normalized digital Doppler shifts  $f_p$ . The system size parameters are  $N = 36$  for the OFDM and AFDM, and  $K = 6, L = 6$  for the OTFS. The fading colors for the fractional Doppler case correspond to the magnitude of the elements whereas darker colors correspond to larger powers. Channel components with a magnitude lower than  $1/2N$  are considered negligible and not visualized in the figure.

#### D. Related Next-Generation Waveforms

In this section, we briefly discuss various waveforms which, as illustrated in Fig. 4 and put into a chronological context in Fig. 5, are related to the aforementioned OFDM, OTFS, and AFDM, and can also be potential candidates to support ISAC in B5G/6G systems. Due to space limitation, however, the discussion is resumed to a qualitative comparison, addressed in more detail in Sec. III.

1) *Intermediate Chirp Domain Waveforms*: A few chirp-domain waveforms also exist, which in commonality with OFDM and AFDM, aim at orthogonalizing delay and Doppler shift indices. Such waveforms, which include orthogonal chirp division multiplexing (OCDM) [10] and DAFT-OFDM [21], can be seen as special cases of AFDM, with non-ideal and simplified chirp frequencies  $c_1$  and  $c_2$  [11], naturally exhibiting equal or worse performances depending on the doubly-dispersive channel profile.

2) *Enhanced Delay-Doppler Waveforms*: Various methods adopt the novel delay-Doppler signal representation of OTFS, and have proposed enhanced delay-Doppler domain waveforms. Examples are the transcendentially-rotated OTFS (T-OTFS) [22], which maximizes the asymptotic diversity of OTFS via a phase-rotating precoder; orthogonal time sequency modulation (OTSM) modulation [23], which seeks to reduce implementation complexity by leveraging a new type of domain transform; and orthogonal delay-Doppler division multiplexing (ODDM) [24], which improves upon OTFS via an optimized pulse-shaping filter that creates feasible pulses that are orthogonal with respect to the delay-Doppler plane resolution.

3) *Filter Bank-based (Pulse-Shaping) Waveforms*: Finally, various multicarrier techniques leverage optimized pulse-shaping filter banks, such as filter bank multi-carrier (FBMC) [25] and generalized frequency division multiplexing (GFDM) [26], which improve the out-of-band (OOB) emissions, spectral efficiency, ISI, and ICI problems of OFDM via robust adaptation of the subcarriers and modulation pulses with respect to the doubly-dispersive channel statistics.

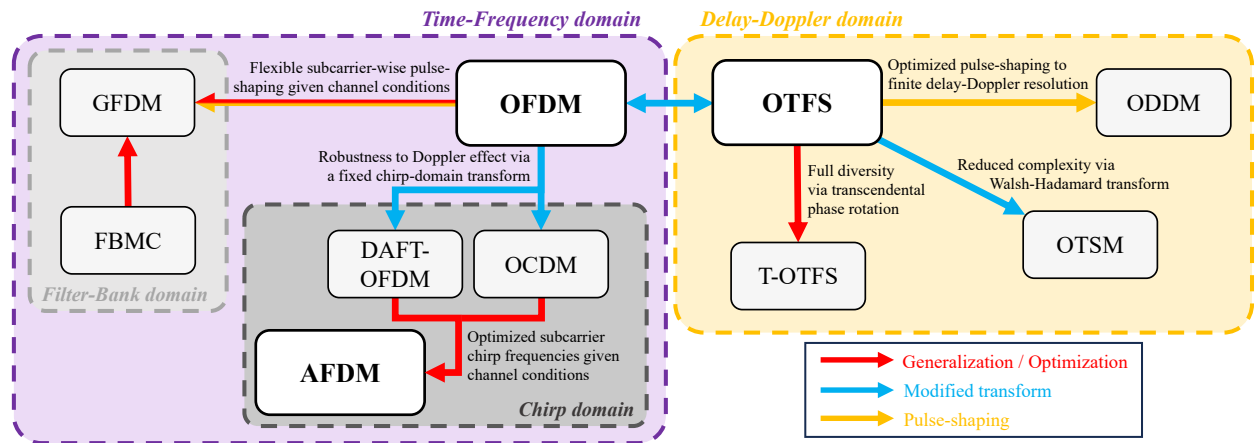


Fig. 4: A map of relationships between next-generation waveforms and their signal domains.



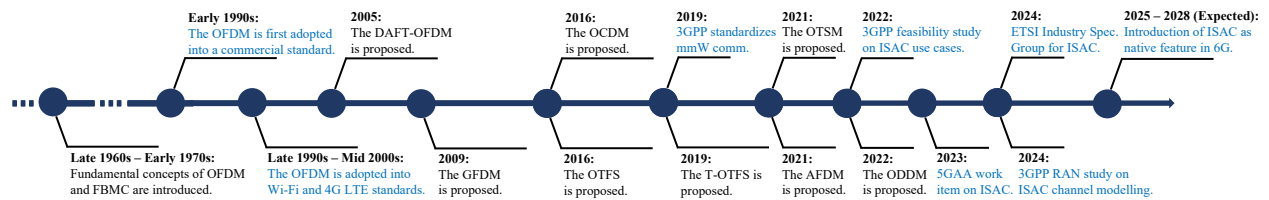


Fig. 5: Timeline highlighting the invention of various waveforms, and key dates in standardization.

#### IV. INTEGRATED SENSING AND COMMUNICATIONS (ISAC) USING NEXT-GENERATION WAVEFORMS

In ISAC, wireless “sensing” refers to the ability to harness the rich information about the surrounding environment inherently embedded in radio signals affected by channel conditions. Drawing a parallel with well-established *radar* technologies [27] two distinct types of sensing problems can therefore be identified, namely: 1) the **detection problem (DP)**, which relates to resolving the number of unique scattering points of interest (targets) from the background clutter, and 2) the **estimation problem (EP)**, which refers to extracting parameters such as range, velocity, and bearing associated with the aforementioned targets. Such sensing scenarios can be classified as monostatic, where the sensing receiver is colocated with the transmitter, or bistatic, where the sensing receiver is spatially remote from the transmitter<sup>16</sup>.

A exemplary ISAC scenario between transmitter and receiver is illustrated in Fig. 6 with a single environment scatterer, where the three sub-scenarios corresponding to the ISAC functionalities and sensing locations can be observed. Namely, there exist both communications and bistatic sensing subsystems between the ISAC transmitter and the ISAC receiver over the same doubly-dispersive channel of the scattering environment, and only the monostatic sensing subsystem for the ISAC transmitter.

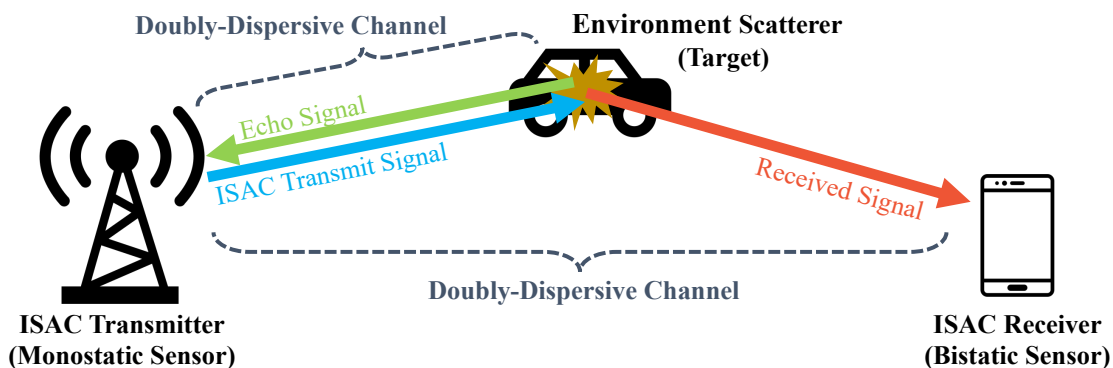


Fig. 6: An illustration of the communications and sensing scenarios involved in an ISAC system.

<sup>16</sup>The bistatic scenario can be further generalized into a multistatic scenario with multiple distributed transmitters and receivers, for several applications and use cases [28]. This scenario is beyond the scope of this article but is an important setting to be addressed in future work, which can enable the full potential of ISAC.

The radar parameters, namely the effective range  $r$  [m] and relative linear velocity  $v$  [m/s] of the target are directly correspondent to the path delay  $\tau$  and Doppler shift  $\nu$  of the target reflected signal,

$$\tau \triangleq \frac{r}{c}, \quad \text{and} \quad \nu \triangleq \frac{2vf_c}{c}, \quad (25)$$

where  $c$  is the speed of light and  $f_c$  is the carrier frequency of the transmitted signal.

For monostatic sensing, the effective range  $r$  is twice the range of the target from the colocated transceiver (round-trip distance), whereas for bistatic scenarios,  $r$  is the sum of the transmitter-to-target and receiver-to-target ranges (total propagation distance). Similarly, for monostatic scenarios, the relative velocity  $v$  is in the direction along a straight line between the target and the transceiver, whereas for bistatic scenarios,  $v$  is in the direction along the bisecting line between the transmitter-to-target and receiver-to-target paths (bistatic velocity).

In light of the relationship in eq. (25), it is important to notice that the fundamental radar target parameters (range and velocity) are equivalent to the path dispersion parameters (delay and Doppler) of the common doubly-dispersive communications channel, as illustrated in Fig. 6.

Solutions to the DPs and EPs can be further classified into **three methods** based on their approaches: a) **correlation-based** methods, in which echo signals are filtered with the known transmit signal in order to yield the radar parameter estimates; b) **direct CSI-based** methods, where radar parameters are extracted *a posteriori* from the known channel matrix; and c) **indirect CSI-based** methods, where radar parameters estimation and channel estimation are performed jointly, by leveraging the known structure of the doubly-dispersive channel of eq. (9). Each of these approaches is discussed further in the sequel.

In the scope of this article, we address only the radar parameter estimation of the SISO model, as the MIMO extension can be trivially derived by leveraging the models in eq. (12) and eq. (13) with the corresponding MIMO radar processing techniques [16]. This enables the estimation of bearing, *i.e.*, the angular direction of the scatterer targets, and in the case of 2D planar arrays, the azimuth and elevation angles of the target in 3D space.

#### A. Correlation-based Methods

Classical radar systems based on chirps and impulsive waveforms [27] are typical examples of the correlation-based method, as the received echo signals are processed by a correlation (matched filter) with a known probing signal, to directly yield the target parameters. Radar waveforms are, however, optimized to exhibit correlation properties that can achieve high resolution in the delay and Doppler domains, which is generally not possible to do with communication waveforms without sacrificing communication objectives (e.g., rate, efficiency, latency, etc.).

The fundamental resolution of the correlation-based method can be analyzed through the well-known 2D ambiguity function of a waveform in delay-Doppler domain<sup>17</sup>, which is given by

$$A(\tau, \nu) \triangleq \int_{-\infty}^{+\infty} s(t) \cdot s^*(t - \tau) \cdot e^{j2\pi\nu t} dt, \quad (26)$$

where  $A(\tau, \nu)$  is the 2D ambiguity function parametrized by the delay and Doppler shift values,  $s(t)$  is the transmit signal, and  $(\cdot)^*$  denotes the complex conjugation operation.

By inspecting the ambiguity function behaviors of the OFDM, OTFS, and AFDM waveforms [29], the different delay-Doppler resolution and beamlobe behaviors of the waveforms can be observed. Namely, it is found that that OFDM shows high resolution in the delay domain, but not in Doppler, whereas OTFS and AFDM show moderate resolution in both domains simultaneously, with AFDM exhibiting an adjustable mainlobe width with a trade-off in the two domains by leveraging the chirp frequency parameters  $c_1$  and  $c_2$ . Therefore naturally, correlation-based estimators of low complexity, employing OFDM, OTFS, and AFDM [29]–[31], have been proposed, but were found to be still fundamentally dependent on the resolution of the ambiguity function, promoting subsequent development of parameter estimation methods based on the higher resolution of the inherent delay-Doppler modulation grid.

Furthermore, it is important to notice that correlation-based methods inherently require the full knowledge of the transmit signal. Therefore, in consideration of the ISAC regime, its application is only feasible for monostatic sensing scenarios in which the transmit signal is fully known, or for bistatic scenarios by leveraging transmission frames with a known sequence, such as a pilot or preamble.

### B. Direct CSI-based Methods

These methods operate under the assumption that channel estimation (CSI acquisition) has already been performed at the ISAC receiver such that the effective channel matrix is available numerically, *i.e.*, as complex taps of the channel matrix, and aim to extract radar parameters *a posteriori* by exploiting the deterministic structure of the doubly-dispersive channel as described in Sec. III. Several sensing algorithms based on this approach have been proposed. Assuming that CSI is obtained in the time-frequency domain as per eq. (2), the resulting estimation problem on  $\tau_p$  and  $\nu_p$  is referred to as a multidimensional harmonic retrieval problem, to which many well-known super-resolution solutions exist, such as MULTiple Signal Classification (MUSIC) and estimation of signal parameters via rotational invariance techniques (ESPRIT), in addition to enhanced tensor-based algorithms in the case of MIMO scenarios with increased dimensionality, as discussed in [6]. The approach is known to achieve high resolution and accuracy but typically requires a large number of continuously obtained observation samples, which together with the

<sup>17</sup>In the case for MIMO, the dimension of the ambiguity function is extended to include the angular domain.

fundamental dependence on the channel estimation performance, constitute a prominent challenge of such methods, since channel estimation errors may propagate to the radar parameter estimates.

Setting these issues aside, with a sufficiently large number of observations and appropriate filtering, the effective channel matrices of the waveforms as given in eqs. (16), (19), and (22) may be obtained via compressive sensing and other matrix reconstruction algorithms. In such cases, the delay-Doppler orthogonality of the OTFS and AFDM effective channels, in addition to the injective mapping between each integer delay-Doppler pair and the position of the shifted-diagonal as discussed in Sec. III, enable efficient extraction of the target parameters from the channel matrix element positions. However, in the presence of fractional Doppler shifts, the resulting interference in the Doppler domain illustrated in Fig. 3b can significantly deteriorate such "position-based" methods in terms of Doppler resolution.

Since the direct CSI-based method inherently assumes the full knowledge of the effective channel matrix, which requires a dedicated channel estimation step involving a known transmit signal, this is also only possible for monostatic sensing scenarios or for bistatic scenarios with a dedicated pilot.

### C. Indirect CSI-based Methods (Integrated Channel Estimation)

In cases where the channel matrix is not available but its structure is known, an estimation problem can be formulated to jointly estimate the channel inherently incorporating the radar parameters, yielding an integrated channel and target parameter estimation. Such scenarios are expected at ISAC receivers where the information of the transmit signal is available but channel estimation has not been performed, or at bistatic ISAC receivers with unknown components of the transmit signal (*i.e.*, information symbols).

When the transmit signal is fully known, the following minimization problem can be solved

$$\underset{\tau_p, \nu_p, h_p, \forall p}{\operatorname{argmin}} \mathcal{L}(\mathbf{y} - \tilde{\mathbf{G}}(\tau_p, \nu_p, h_p; \forall p) \cdot \mathbf{x}), \quad (27)$$

where  $\mathbf{y} \triangleq \mathbf{G}\mathbf{s} + \mathbf{w} \in \mathbb{C}^{N \times 1}$  is the demodulated received signal where  $\mathbf{G}$  is the effective channel corresponding to the specific waveform,  $\tilde{\mathbf{G}}(\tau_p, \nu_p, h_p; \forall p) \in \mathbb{C}^{N \times N}$  is the estimated effective channel parametrized by the  $3P$  parameters  $\tau_p, \nu_p, h_p$  for  $p \in \{1, \dots, P\}$ , and  $\mathbf{s} \in \mathbb{C}^{N \times 1}$  is the transmit symbol vector, and  $\mathcal{L}(\cdot)$  is an arbitrary objective function, *i.e.*, the  $L_2$  norm.

In the doubly-dispersive case, the parametrized channel  $\tilde{\mathbf{H}}$  is given by eq. (9), or pre-processed via leveraging the effective channel models of specific waveforms described, *e.g.*, by eqs. (16), (19), or (22) for OFDM, OTFS and AFDM, respectively.

On the otherhand, when parts of the transmit signal is also unknown, a bilinear estimation is required

in the form of a joint channel and data estimation (JCDE) problem on the system described by

$$\mathbf{y} = \tilde{\mathbf{G}}(\tau_p, \nu_p, h_p; \forall p) \cdot \tilde{\mathbf{x}} \in \mathbb{C}^{N \times 1}, \quad (28)$$

where  $\mathbf{y} \in \mathbb{C}^{N \times 1}$  is the demodulated received signal,  $\tilde{\mathbf{G}}(\tau_p, \nu_p, h_p; \forall p) \in \mathbb{C}^{N \times N}$  is the estimated effective channel matrix parametrized by the  $3P$  parameters,  $\tilde{\mathbf{x}} \triangleq \mathbb{C}^{N \times N}$  is the estimated transmit symbol vector composed of known pilot symbols and unknown information symbols.

The joint estimation of the unknown data symbols and the unknown channel parametrized by the  $3P$  radar parameters, is therefore an inherently equivalent problem to the joint target detection and data estimation, which can be solved via a plethora of methods as will be elaborated in the following section.

#### D. Estimation Methods of CSI-based Methods

There are largely two approaches to the underlying  $3P$ -parameter estimation problem present in CSI matrix-based sensing methods in Sections IV-B and IV-C: *a)* on-grid search-based methods which yield values corresponding to the resolution of the discretized parameter grid, and *b)* off-grid methods which directly yield a continuous estimate of the parameters.

On-grid methods [32], [33] assume the domain of the path delay and Doppler shift to be discrete on a given grid resolution, typically of the discretely sampled signal and channel, and solve the optimization problem via maximum likelihood (ML), *i.e.*, a search over the discrete parameter solution space. Typically, the parameter grid is initially limited to the sampling frequency, which are the integer values of the normalized delay and normalized digital Doppler frequency. However, a common approach is to first obtain the on-grid "coarse" integer estimates of the parameters, then perform an iterative search around the estimate with a virtually sub-divided grid. Such sub-divisions can be refined to arbitrarily high resolutions, but trivially require a higher complexity as the estimation requires the optimization over the sub-divided grid is still discrete.

On the other hand, off-grid methods directly yield a continuous estimate of the radar parameters by leveraging a variety of techniques methods including message passing, Bayesian learning, convex optimization, harmonic retrieval, *etc.*, [34], [35]. Such methods are not restricted by the resolution of the sampling frequency or a discrete grid, and capable of directly estimating the fractional components of the parameters, but as they are not ML, may be more prone to the error caused by the noise and interference, and may exhibit an algorithmic resolution limit (*i.e.*, error-floor).

## V. KEY PERFORMANCE INDICATOR (KPI)-CENTERED COMPARATIVE ANALYSIS

In view of all the above, we finally offer a qualitative comparison of OFDM, OTFS and AFDM – respectively representing the classic, SotA and most-recent alternative – ISAC-friendly waveforms for B5G/6G systems. To this end, we consider various relevant KPIs for communication and sensing, functions, both in terms of features and implementation aspects. The GFDM and FMCW waveforms are also included for comparison, for communications and radar sensing performances respectively.

The result is given in Table I, and while it is not possible to elaborate on all comparison points due to space limitations, we briefly elaborate on a few most important of the selected KPIs. In particular, perhaps the most important communications KPI in doubly-dispersive channels is the Doppler-shift robustness, *i.e.*, the compatibility to high-mobility and EHF conditions, which is only attained by the OTFS and AFDM waveforms due to the inherent delay-Doppler domain orthogonality. On this aspect, it is noteworthy than

TABLE I: A comparative table of various waveforms and their ISAC KPIs, with qualitative measures: high, medium, low. The color of each cell corresponds to the relative performance measure, ranging from **green** denoting an attractive performance, **yellow**, to **red** denoting less performant.

		Key Performance Indicator	Waveform			
			OFDM	OTFS	AFDM	GFDM
Communications	Performance	Waveform Domain	Time-frequency	Delay-Doppler	Chirp	Filter-bank
		Delay Robustness	High	High	High	High
		Doppler Robustness	Low	High	High	Medium
		Peak-to-Average Power Ratio	High	Low	High	Medium
		Diversity in TV Channels	Low	Medium	High	Medium
		Frame Guard (CP) Overhead	High	Low	Medium	Medium
		Pilot Guard Overhead	Medium	High	Low	Medium
	Implementation	Modulation Complexity	Low	High	Medium	High
		OFDM Compatibility	High	High	High	High
		Power amplifier (PA) Strain	High	Low	High	Medium
		MIMO Scalability	High	Medium	High	Medium
		EHF Feasibility	Low	High	High	Medium
		Full-Duplex Potential	Low	Medium	High	Medium
		Key Performance Indicator	OFDM	OTFS	AFDM	FMCW
Target Sensing	Performance	Delay Ambiguity	Low	Medium	Variable	Low
		Doppler Ambiguity	High	Medium	Variable	Low
		Peak-to-Sidelobe Ratio	Medium	Low	Variable	Low
		Max. Unambiguous Range	Medium	Medium	Medium	High
		Max. Unambiguous Velocity	Medium	Medium	Medium	High
	Implem.	Implementation Cost	Low	Medium	Medium	Low
		Engineering Complexity	Low	Medium	Medium	Low
		MIMO Array Extendibility	High	Medium	High	High
		ISAC Feasibility	Medium	High	High	Medium

OTFS achieves full diversity only in finite signal-to-noise ratio (SNR) regimes converging to first order asymptotic diversity [22], while AFDM provides guaranteed full diversity generally [11] and is also known to be the only Doppler-robust waveform to achieve full diversity also in MIMO scenarios. On the other hand, due to their fundamental roots on OFDM, both AFDM and GFDM also suffer from higher peak-to-average power ratio (PAPR), whereas OTFS enjoys a low PAPR due to the DFT-based spreading of the symbol powers in the time-frequency domain. This advantage is closely linked to implementation cost and hardware stability, especially in relation to the PA and radio frequency (RF) component efficiency which becomes more prominent in the massive MIMO scenarios.

Another important point to consider is the computational complexity, which is linked to various signal processing procedures such as modulation and channel estimation. In this regard, while both OTFS and AFDM can be interpreted as modified precoding schemes for OFDM transmitters, such that core OFDM modulators can be reused, the one-dimensional (1D) AFDM modulator exhibits a higher efficiency than the 2D OTFS modulator. This reduced dimension of the waveform also shows a similar advantage for channel estimation, in terms of both computational complexity and the required piloting overhead.

In terms of target sensing performance, OTFS and AFDM exhibit a significant improvement in the Doppler-domain ambiguity over OFDM, but such methods are restricted as they are not optimized for correlation as with FMCW waveforms. Therefore, super-resolution methods and on-grid estimation methods on the discrete delay-Doppler domain of the waveforms are leveraged, which can achieve extremely high resolutions compared to those of FMCW, often used in automotive radar, given sufficient parameterization such as the carrier frequency and symbol period.

The above-described properties in both communications and sensing performances must be satisfied and be coherent, in order for a waveform to be considered a strong candidate for ISAC in B5G/6G. Clearly, as observed from the color scaling of Table. I, OTFS and AFDM are the most promising candidates satisfying most of the ISAC criteria, with some trade-offs between the two waveforms in terms of complexity, power and spectral efficiency, which is to be further addressed in a future work.

## VI. FUTURE WORKS

It can be seen that while OTFS and AFDM are the most promising candidates to enable high-performance ISAC for next-generation wireless networks, there are still many important topics to be addressed in order to enable the incorporation of such techniques into future standards. Indeed, any given row of Table I – such as the PAPR of AFDM or the CSI estimation complexity of OTFS – can be a subject of optimization and development. The authors hope that this article helps the ISAC research community with fundamental insights, techniques, and future direction to promote the development

of high-performance ISAC in doubly-dispersive environments for next-generation wireless networks. Furthermore, in light of the consolidated fundamentals and the identification of potentials and challenges of the doubly-dispersive environment and the promising waveforms, it is also important to investigate the implications towards the consequent practical implementations and design.

## REFERENCES

- [1] T. S. Rappaport, Y. Xing, O. Kanhere, S. Ju, A. Madanayake, S. Mandal, A. Alkhateeb, and G. C. Trichopoulos, "Wireless communications and applications above 100 GHz: Opportunities and challenges for 6G and beyond," *IEEE Access*, vol. 7, pp. 78 729–78 757, 2019.
- [2] N.-S. Vo, T. Q. Duong, and Z. Sheng, "The key trends in B5G technologies, services and applications," *Mobile Networks and Applications*, vol. 27, no. 4, pp. 1716–1718, 2022.
- [3] Y. Zhong, T. Bi, J. Wang, J. Zeng, Y. Huang, T. Jiang, Q. Wu, and S. Wu, "Empowering the V2X network by integrated sensing and communications: Background, design, advances, and opportunities," *IEEE Network*, vol. 36, no. 4, pp. 54–60, 2022.
- [4] D. W. Bliss and S. Govindasamy, *Dispersive and doubly dispersive channels*. Cambridge University Press, 2013, pp. 341–364.
- [5] T. Wang, J. Proakis, E. Masry, and J. Zeidler, "Performance degradation of OFDM systems due to doppler spreading," *IEEE Transactions on Wireless Communications*, vol. 5, no. 6, pp. 1422–1432, 2006.
- [6] J. A. Zhang, M. L. Rahman, K. Wu, X. Huang, Y. J. Guo, S. Chen, and J. Yuan, "Enabling joint communication and radar sensing in mobile networks—a survey," *IEEE Commun. Surveys Tuts.*, vol. 24, no. 1, pp. 306–345, 2022.
- [7] Z. Wei, W. Yuan, S. Li, J. Yuan, G. Bharatula, R. Hadani, and L. Hanzo, "Orthogonal time-frequency space modulation: A promising next-generation waveform," *IEEE Wireless Communications*, vol. 28, no. 4, pp. 136–144, 2021.
- [8] W. Anwar, A. Krause, A. Kumar, N. Franchi, and G. P. Fettweis, "Performance analysis of various waveforms and coding schemes in V2X communication scenarios," in *2020 IEEE Wireless Communications and Networking Conference (WCNC)*, 2020, pp. 1–8.
- [9] L. Gaudio, M. Kobayashi, G. Caire, and G. Colavolpe, "On the effectiveness of OTFS for joint radar parameter estimation and communication," *IEEE Transactions on Wireless Communications*, vol. 19, no. 9, pp. 5951–5965, 2020.
- [10] X. Ouyang and J. Zhao, "Orthogonal chirp division multiplexing," *IEEE Transactions on Communications*, vol. 64, no. 9, pp. 3946–3957, 2016.
- [11] A. Bemani, N. Ksairi, and M. Kountouris, "Affine frequency division multiplexing for next generation wireless communications," *IEEE Transactions on Wireless Communications*, pp. 1–1, 2023.
- [12] J. J. Healy, M. A. Kutay, H. M. Ozaktas, and J. T. Sheridan, *Linear canonical transforms: Theory and applications*. Springer, 2015, vol. 198.
- [13] Nokia, Nokia Shanghai Bell, "RP-234069: Study on channel modelling for Integrated Sensing And Communication (ISAC) for NR," Tech. Rep., dec 2023, RAN Meeting #102.
- [14] Y. Hong, T. Thaj, and E. Viterbo, *Delay-Doppler Communications: Principles and Applications*. Academic Press, 2022.
- [15] ETSI, "ETSI TR 125 996 V17.0.0 - Universal Mobile Telecommunications System (UMTS); Spatial channel model for Multiple Input Multiple Output (MIMO) simulations (3GPP TR 25.996 version 17.0.0 Release 17)," Tech. Rep., 2022.
- [16] J. Li and P. Stoica, *MIMO radar signal processing*. John Wiley & Sons, 2008.
- [17] R. Prasad, *OFDM for wireless communications systems*. Artech House, 2004.



- [18] V. S. Bhat, G. Harshvardhan, and A. Chockalingam, "Input-output relation and performance of RIS-aided OTFS with fractional delay-doppler," *IEEE Communications Letters*, vol. 27, no. 1, pp. 337–341, 2023.
- [19] Z. Wei, W. Yuan, S. Li, J. Yuan, and D. W. K. Ng, "Transmitter and receiver window designs for orthogonal time-frequency space modulation," *IEEE Transactions on Communications*, vol. 69, no. 4, pp. 2207–2223, 2021.
- [20] S.-C. Pei and J.-J. Ding, "Closed-form discrete fractional and affine fourier transforms," *IEEE transactions on signal processing*, vol. 48, no. 5, pp. 1338–1353, 2000.
- [21] T. Erseghe, N. Laurenti, and V. Cellini, "A multicarrier architecture based upon the affine fourier transform," *IEEE Transactions on Communications*, vol. 53, no. 5, pp. 853–862, 2005.
- [22] G. D. Surabhi, R. M. Augustine, and A. Chockalingam, "On the diversity of uncoded OTFS modulation in doubly-dispersive channels," *IEEE Transactions on Wireless Communications*, vol. 18, no. 6, pp. 3049–3063, 2019.
- [23] T. Thaj, E. Viterbo, and Y. Hong, "Orthogonal time sequency multiplexing modulation: Analysis and low-complexity receiver design," *IEEE Transactions on Wireless Communications*, vol. 20, no. 12, pp. 7842–7855, 2021.
- [24] H. Lin and J. Yuan, "Orthogonal delay-doppler division multiplexing modulation," *IEEE Transactions on Wireless Communications*, vol. 21, no. 12, pp. 11 024–11 037, 2022.
- [25] B. Farhang-Boroujeny, "OFDM versus filter bank multicarrier," *IEEE signal processing magazine*, vol. 28, no. 3, pp. 92–112, 2011.
- [26] N. Michailow, M. Matthé, I. S. Gaspar, A. N. Caldevilla, L. L. Mendes, A. Festag, and G. Fettweis, "Generalized frequency division multiplexing for 5th generation cellular networks," *IEEE Transactions on Communications*, vol. 62, no. 9, pp. 3045–3061, 2014.
- [27] M. A. Richards, *Fundamentals of Radar Signal Processing*. |country;US|/country;: McGraw-Hill Professional, 2005. [Online]. Available: <https://mhbooklibrary.com/doi/book/10.1036/0071444742>
- [28] H. S. Rou, G. T. Freitas de Abreu, D. González G., and O. Gonsa, "Integrated sensing and communications for 3D object imaging via bilinear inference," *Accepted at the IEEE Transactions on Wireless Communications*, 2024.
- [29] J. Zhu, Y. Tang, X. Wei, H. Yin, J. Du, Z. Wang, and Y. Liu, "A low-complexity radar system based on affine frequency division multiplexing modulation," *arXiv preprint arXiv:2312.11125*, 2023.
- [30] P. Kumari, J. Choi, N. González-Prelcic, and R. W. Heath, "IEE 802.11ad-based radar: An approach to joint vehicular communication-radar system," *IEEE Transactions on Vehicular Technology*, vol. 67, no. 4, pp. 3012–3027, 2018.
- [31] P. Raviteja, K. T. Phan, Y. Hong, and E. Viterbo, "Orthogonal time frequency space (OTFS) modulation based radar system," in *2019 IEEE Radar Conference (RadarConf)*, 2019, pp. 1–6.
- [32] M. F. Keskin, H. Wymeersch, and A. Alvarado, "Radar sensing with OTFS: Embracing ISI and ICI to surpass the ambiguity barrier," in *2021 IEEE International Conference on Communications Workshops (ICC Workshops)*, 2021, pp. 1–6.
- [33] K. R. R. Ranasinghe, H. S. Rou, and G. T. F. de Abreu, "Fast and efficient sequential radar parameter estimation in MIMO-OTFS systems," in *ICASSP 2024 - 2024 IEEE International Conference on Acoustics, Speech and Signal Processing (ICASSP)*, 2024.
- [34] C. Liu, S. Liu, Z. Mao, Y. Huang, and H. Wang, "Low-complexity parameter learning for OTFS modulation based automotive radar," in *ICASSP 2021 - 2021 IEEE International Conference on Acoustics, Speech and Signal Processing (ICASSP)*, 2021, pp. 8208–8212.
- [35] Z. Wei, W. Yuan, S. Li, J. Yuan, and D. W. K. Ng, "Off-grid channel estimation with sparse bayesian learning for OTFS systems," *IEEE Transactions on Wireless Communications*, vol. 21, no. 9, pp. 7407–7426, 2022.